Research article

Moritz Merklein*, Birgit Stiller, Khu Vu, Pan Ma, Stephen J. Madden and Benjamin J. Eggleton

On-chip broadband nonreciprocal light storage

Abstract: Breaking the symmetry between forward- and backward-propagating optical modes is of fundamental scientific interest and enables crucial functionalities, such as isolators, circulators, and duplex communication systems. Although there has been progress in achieving optical isolation on-chip, integrated broadband nonreciprocal signal processing functionalities that enable transmitting and receiving via the same low-loss planar waveguide, without altering the frequency or mode of the signal, remain elusive. Here, we demonstrate a nonreciprocal delay scheme based on the unidirectional transfer of optical data pulses to acoustic waves in a chip-based integration platform. We experimentally demonstrate that this scheme is not impacted by simultaneously counter-propagating optical signals. Furthermore, we achieve a bandwidth more than an order of magnitude broader than the intrinsic optoacoustic linewidth, linear operation for a wide range of signal powers, and importantly, show that this scheme is wavelength preserving and avoids complicated multimode structures.

Moritz Merklein and Birgit Stiller have contributed equally to this work.

*Corresponding author: Moritz Merklein, The University of Sydney Nano Institute (Sydney Nano), The University of Sydney, Sydney, NSW 2006, Australia; and Institute of Photonics and Optical Science (IPOS), School of Physics, The University of Sydney, Sydney, NSW 2006, Australia, E-mail: moritz.merklein@sydney.edu.au. https://orcid.org/0000-0002-5558-2592
Birgit Stiller, The University of Sydney Nano Institute (Sydney Nano), The University of Sydney, Sydney, NSW 2006, Australia; Institute of Photonics and Optical Science (IPOS), School of Physics, The University of Sydney, Sydney, NSW 2006, Australia; and Max-Planck-Institute for the Science of Light, Staudtstr. 2, 91058 Erlangen, Germany
Khu Vu and Stephen J. Madden, Max-Planck-Institute for the Science of Light, Staudtstr. 2, 91058 Erlangen, Germany
Pan Ma, Laser Physics Centre, Research School of Physics and Engineering, Australian National University, Canberra, ACT 2601, Australia
Benjamin J. Eggleton, The University of Sydney Nano Institute (Sydney Nano), The University of Sydney, Sydney, NSW 2006, Australia; and Institute of Photonics and Optical Science (IPOS), School of Physics, The University of Sydney, Sydney, NSW 2006, Australia

1 Introduction

Reciprocity is a general concept in optics dictating that a transmission channel does not change, or is symmetric, under the interchange of source and receiver [1–3]. There are, however, different approaches to break this reciprocity, most commonly by utilizing magnetic materials [4–6]. The arguably most common devices based on breaking reciprocity are isolators utilizing magnetic materials. Isolators based on magnetic materials are passive components and have large bandwidth and rejection. Chip integration and material losses, however, are still major challenges despite the great progress made over the recent years.

Another way to achieve nonreciprocal transmission is based on temporal modulation [2, 7]. Although this active method requires some sort of pumping – electrical [8], optical [9], or acoustic [10] – it offers great potential as it does not rely on magnetic materials and hence is more suitable for chip integration with the additional advantage of being reconfigurable. Nonreciprocal elements, such as optical isolators and circulators are crucial building blocks, in particular, for integrated photonic circuits to protect the laser but also to route counterpropagating signals and mitigate back-reflections that can arise from boundaries between multiple elements or are simply caused by Rayleigh backscattering.

A powerful and versatile way to achieve nonreciprocal transmission in a small footprint can be realized by coupling light and mechanical degrees of freedom [11, 12]. This coupling between light and mechanical oscillations is greatly enhanced in resonant structures which lead to demonstrations of chip-scale optomechanical isolators and circulators for optical [13–19] as well as microwave signals [20–23].

Similarly, stimulated Brillouin scattering (SBS), i.e. the resonant coupling of optical waves with propagating acoustic waves in waveguides via optically induced forces is known to be nonreciprocal [9, 24]. The phase-matching

condition ensures that only pump and probe waves which are counterpropagating (copropagating) couple to the acoustic wave which is mainly longitudinal for backward SBS (transverse for forward Brillouin scattering) [25]. As these acoustic waves carry momentum, Brillouin interactions can be used to induce indirect photonic transitions between different optical modes [9, 24, 26].

Numerous experiments have reported nonreciprocity exploiting Brillouin interactions, including demonstrations in photonic crystal fibers [9], silicon waveguides [27], and fiber-tip resonators [28–30]. Surprisingly, however, so far there was no demonstration of Brillouin-based nonreciprocal schemes harnessing backward SBS. In this approach, the optical wave can couple to a continuum of acoustic modes that provides enormous flexibility, which is particularly important for nonreciprocal signal processing schemes that go beyond providing pure signal isolation. Furthermore, large backward SBS gain can be achieved in small footprint planar integrated circuits [25].

Here, we show a nonreciprocal light storage scheme based on coherent Brillouin coupling of acoustic and optical modes to achieve nonreciprocal delay. We experimentally demonstrate that optical pulses that are traveling simultaneously in the opposite direction, with the same optical frequency and mode, are not impacted nor do they impact the storage process. We show that the bandwidth of the scheme can be broadened beyond the intrinsic acoustic linewidth – in this demonstration by more than one order of magnitude – which was generally thought to be a limiting factor of SBS-based nonreciprocal schemes. Furthermore, the scheme depends linearly on the input data pulse power in the observed range and does neither alter the frequency nor mode of the incoming data – all important requirements for practical nonreciprocal devices.

2 Results

The nonreciprocity is induced by an interaction between two counterpropagating optical modes – here we call them data ω_{data} and write/read $\omega_{\text{w/r}}$ – with a traveling acoustic mode Ω. To enable efficient coupling from optical to acoustic waves, the optical write/read and the data pulses are separated by the frequency of the acoustic wave in the waveguide, known as the Brillouin frequency shift, $\Omega = 2 \cdot n_{\text{eff}} \cdot v_{\text{ac}} \cdot \lambda^{-1}$, where n_{eff} is the effective refractive index, v_{ac} the acoustic sound velocity in the material, and λ the optical pump wavelength. The waveguide used in this demonstration is made out of chalcogenide glass and the corresponding acoustic resonance frequency is $\Omega \approx 7.6$ GHz. The underlying physical mechanisms that

couple the two optical and the acoustic waves are electrostriction – the compression of a material in regions of strong light fields and photoelasticity – the change of refractive index with material density [31].

Brillouin interactions can be used to store optical data pulses as acoustic waves on a photonic chip [32]. The optical data pulses are frequency-upshifted from counterpropagating write and read pulses by precisely the Brillouin frequency shift Ω. Hence, the optical data pulses are first depleted by the write pulses and an acoustic wave is generated and are later retrieved using read pulses which deplete the acoustic wave.

This interaction has not only to fulfill energy conservation $\omega_{\text{data}} = \omega_{\text{w/r}} + \Omega$ but also momentum conservation $\mathbf{k}_{\text{data}} = \mathbf{k}_{\text{w/r}} + \mathbf{q}$. As the momentum $\mathbf{q}$ of the traveling acoustic wave in backward SBS is large, approximately twice the magnitude of the momentum vectors of the individual optical modes $|\mathbf{q}| \approx 2 \cdot |\mathbf{k}_{\text{data}}|$ with $|\mathbf{k}_{\text{data}}| \approx |\mathbf{k}_{\text{w/r}}|$, the interaction is only phase-matched in one direction. Note that the phase-matching condition for exciting an acoustic wave with a particular pair of counterpropagating optical pulses can always be fulfilled by matching the detuning to the Brillouin frequency shift in the waveguide as opposed to interdigitated transducer–based approaches that require careful device design and fabrication to ensure phase-matching is fulfilled [10].

That the Brillouin process is only phase-matched for data signals traveling in one direction becomes more evident when looking at the dispersion diagram shown in Figure 1a, where changing the direction of one optical mode leads to a phase mismatch $\Delta\mathbf{q}$. As the interaction takes place over an elongated length given by either the length of the waveguide, for the case of continuous wave (CW) signals, or the length of the optical signal pulse, a small initial phase mismatch builds up to a large mismatch over that interaction length as it was shown for the case of Brillouin interactions that involve multiple optical wavelengths [33]. Even in the case of nanosecond (ns) and subnanosecond pulses, this length scale is in the order of several centimeters.

How this strict phase-matching condition of the optoacoustic Brillouin interaction can be utilized to achieve unidirectional signal delays is shown in Figure 1b. Optical data pulses ω_{data} that propagate from the left through the waveguide are transferred to acoustic phonons via a Brillouin interaction induced by counterpropagating write pulses ω_{w} and are subsequently retrieved using read pulses ω_{r} [32, 34, 35], whereas optical pulses that travel in the opposite direction are neither effected by the write, the read pulses nor the acoustic wave that stores the original optical pulses ω_{data}. The phase-matching condition
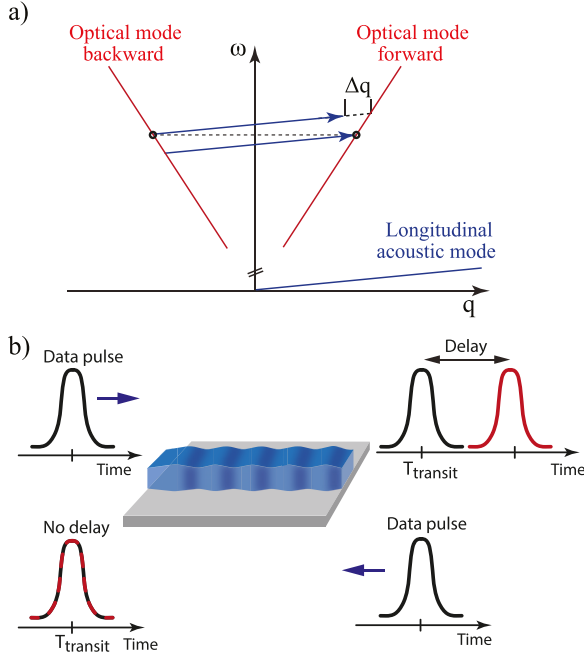
a)

b)

Figure 1: Basic principle and phase-matching diagram.
(a) Dispersion diagram for backward Brillouin scattering illustrating the phase-matching condition for data pulses propagating in opposite directions. (b) Optical data pulses that are coupled from the left side into the waveguide are converted to acoustic phonons and experience a delay. Optical data pulses that are coupled simultaneously from the opposite side in the waveguide do not experience any conversion and hence are not delayed.

between the optical modes and the traveling acoustic wave ensures that there is no interaction, even for the extreme case when the counterpropagating optical pulses are in the same optical waveguide mode, at the same frequency and optical power.

Data pulses that are transferred to the acoustic domain accumulate a large delay because of the five orders of magnitude difference in velocity between the acoustic and optical waves. The accumulated delay of the optical signal can hence be approximated by the time difference between the writing and the retrieving operation. Thus, the delay of the optical signal can be continuously tuned within the acoustic lifetime of the acoustic phonon that is given by the material properties of the chalcogenide glass and is in the order of 10 ns [32].

Owing to the phase-matching condition of the Brillouin interaction, the coupling between optical and acoustic wave only occurs for a certain pair of optical write/ read and data pulses. Optical data pulses that are simultaneously propagating through the waveguide from the opposite side are neither transferred to the acoustic wave by the write pulses, nor do they interact with the acoustic wave present in the waveguide and hence do also not

influence the stored data pulses. The counterpropagating signals could be data pulses that are simultaneously transmitted/received in the opposite direction through the same waveguide or could simply originate from backscattering in the photonic circuit.

2.1 Experimental setup

The simplified experimental setup is shown in Figure 2 (a detailed scheme and description can be found in Section 4). A CW distributed feedback laser is split into two paths, the data and the write/read path. The data signal is shifted by the Brillouin frequency shift Ω of the waveguide. Afterward, the CW signals in both arms are modulated into short pulses using a multichannel arbitrary waveform generator and electro-optic intensity modulators. The data signal is split using a 50/50 coupler. One part of the signal is combined with the write/read arm and coupled to the nonlinear chalcogenide waveguide. The other half passes through an additional 50/50 coupler, to ensure that the path length of both data signals as well as their optical power is the same in both arms, and is coupled to the chalcogenide chip from the opposite side. On both sides of the chip circulators are used to separate input and output. Two narrowband filters (bandwidth $\approx$ 3 GHz) are used to separate the data signal from the pump signal and fast photodetectors (bandwidth > 10 GHz) and a fast oscilloscope (bandwidth > 10 GHz) are used to detect the data pulses. A cross-section of the chalcogenide waveguides is shown in the inset of Figure 2. A rib structure with a cross-section of 2200×850 nm^2 is used to reduce losses caused by sidewall roughness. The chalcogenide glass is surrounded by silica glass to ensure confinement of the optical as well as the acoustic mode [36]. For details on the fabrication of the acousto-optic waveguides, see Section 4. The simulated dispersion of the waveguide for both optical modes (forward and backward) is around –200 ps/nm/km. Although it is larger than in standard single-mode fiber, for the length of the chip (22 cm) and the bandwidth of the pulses (around 4 pm), the signal distortion from dispersion is negligible.

2.2 Nonreciprocal Brillouin light storage

Figure 3a shows the transfer of an optical data pulse ω_{data} to an acoustic wave by a counterpropagating write pulse ω_w (black curve; full-width half-maximum $\approx$ 1 ns). The depleted optical signal is shown in red (Figure 3a). Around 90% of data pulse depletion could be achieved, whereas a simultaneously counterpropagating data pulse
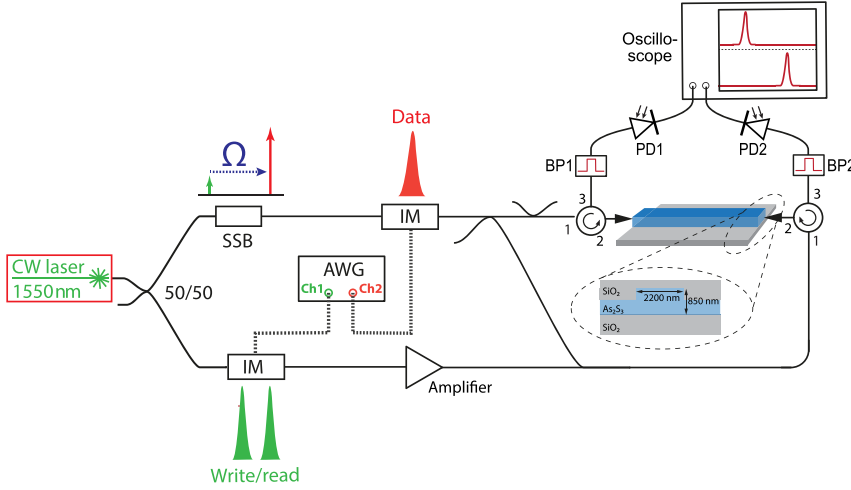
Figure 2: Schematic experimental setup. Continuous wave (CW) laser, continuous wave distributed feedback (DFB) laser; 50/50 fiber coupler; SSB, single-sideband modulator; IM, intensity modulator; AWG, multichannel arbitrary waveform generator; Amplifier, erbium-doped fiber amplifier; BP, bandpass filter; PD, photodetector. Inset: cross-section of the chalcogenide rib waveguide embedded in silica.

(copropagating to the write pulses) is not impacted by the acoustic wave generated in the depletion process (inset Figure 3a). The black curve in the inset shows optical data pulses transmitted in the counterpropagating direction, whereas there is no data transferred to the acoustic wave. The red dashed curve in the inset of Figure 3a shows the counterpropagating optical data pulses while the data traveling in the opposite direction is depleted and transferred to a traveling acoustic wave. Both curves perfectly overlap. In the current experimental implementation, the depletion efficiency of 90% was mainly limited by power constraints and can in principle reach almost full conversion of the optical pulse to the acoustic wave. Figure 3b shows the fast Fourier transform (FFT) of the optical input data pulses demonstrating that the bandwidth of the optical data pulses that can be successfully depleted and transferred to the acoustic domain can greatly exceed the intrinsic Brillouin linewidth of 30 MHz. The dashed lines in Figure 3b indicate the full-width half-maximum of the FFT of the data pulses.

This extension of the bandwidth by more than one order of magnitude beyond the intrinsic acoustic linewidth is enabled by the ultrahigh Brillouin gain provided in chalcogenide waveguides which is about two orders of magnitude larger than in standard silica single-mode fiber. The strength of the interaction is usually measured in terms of Brillouin gain G which gives the amplification of the Stokes wave for a given pump power P and is proportional to $\propto \exp(g\, L_{\mathrm{eff}}\, P)$, with $g = g_0 \cdot A_{\mathrm{AO}}^{-1}$ given by the Brillouin gain coefficient g_0 and the acousto-optic area A_{AO}, and L_{eff} being the effective length. If the pump is broadened beyond the 30 MHz intrinsic linewidth of the Brillouin interaction, more overall pump power is required. As in this experiment, the effective length L_{eff} is limited to the interaction length of the counterpropagating short pulses (cm –
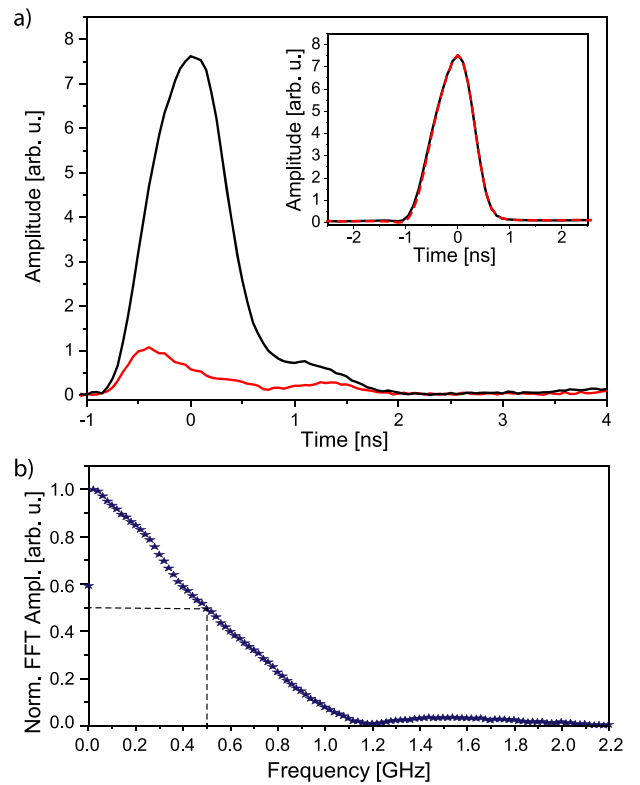

Figure 3: Nonreciprocal pulse depletion.
(a) Conversion of an optical data pulse (black curve) to acoustic phonons (red curve) while a simultaneously counterpropagating data pulse is not impacted (black and dashed red curve in inset). (b) Fast Fourier transform (FFT) of the input data pulse.

tens of cm range), a large gain factor g is required to achieve broad bandwidth operation. For our chips, the Brillouin gain coefficient was previously measured to be $g_0 \approx 0.715 \times 10^{-9}$ m/W and the acousto-optic area $A_{\mathrm{AO}} \approx 1.5\ \mu\mathrm{m}^2$ that leads to the approximately two orders of magnitude increase in the Brillouin factor g [37].

The broad bandwidth is one main advantage of the resonator-free waveguide-based Brillouin approach. Although the intrinsic linewidth of the optoacoustic interaction is given by the phonon lifetime for a single frequency CW optical pump the Brillouin response can be broadened by using a broad bandwidth optical pump where the bandwidth of the Brillouin response is then given by the bandwidth of the optical pump itself. The intrinsic Brillouin gain is in this case distributed over the bandwidth and hence the absolute maximum Brillouin gain is reduced accordingly for a given input power.

After demonstrating the nonreciprocal depletion of optical data pulses, we now show that we can retrieve the data back from the acoustic to the optical domain, even in the presence of counterpropagating pulses, and hence unidirectionally delay optical signals relative to the regular transit time of the waveguide. Figure 4a shows experimental measurements of a 1 ns long optical data pulse that is delayed by 4 ns when propagating in one direction in the waveguide, whereas an optical data pulse simultaneously propagating in the opposite direction with the same optical frequency and optical mode is not interacting with the Brillouin storage process or the acoustic wave present in the waveguide (Figure 4). The transit time of the chip is around 1.8 ns and hence our measured delay would equate to an increase in the group index by a factor of about 2.2. As a proof-of-principle demonstration, we only show a pulse delay of 4 ns; however, we note that the delay is given by the arrival time difference between the write and the read pulses and hence can continuously be tuned. As the phonon exponentially decays as e^{-2t/τ_A}, with τ_A being the acoustic lifetime, the readout efficiency decreases for longer storage times. The phonon lifetime in our waveguide structure is mainly limited by the properties of the chalcogenide material. Much longer phonon lifetimes have been shown in acoustic resonators that hence could achieve longer storage times, however, at the expense of the bandwidth [29, 38, 39]. Furthermore, the shape of the pulses is challenging to be maintained in resonator-based acoustic light storage with the spatial extent of the pulses exceeding the circumference of the resonators.

Conversely, in the here-demonstrated delay scheme, the pulse shape is maintained (Figure 4a). The input data pulse and the delayed data pulse in Figure 4a are normalized to visually emphasize that point and show the similarity in the pulse shape as it is a common practice for fiber-based optical pulse delay techniques [35, 40–44]. The readout efficiency of this measurement was around 20% after a delay of 4 ns. Here, the efficiency is slightly below the record of 32% after a delay time of 3.5 ns reported previously [32], which can be accounted to overall power limitations of the experimental setup due to simultaneously counterpropagating signals.

While the data pulses are stored and delayed in one direction, simultaneously counterpropagating data pulses are not delayed (Figure 4b). The black curve in Figure 4b shows an optical pulse when there is no delay applied to the data that travels in the opposite direction, whereas the dashed red curve shows the optical pulse for the case when the counterpropagating channel is delayed via coherent transfer from optical to acoustic and back to the optical domain. Here, the data pulses are not normalized to emphasize that there is neither a change in amplitude nor shape of the pulses. The counterpropagating data pulses do not interact with the acoustic mode present in the waveguide from the delay process of the data pulses propagating in the opposite direction nor do they distort the storage process of these pulses. Hence, we show that the nonreciprocal pulse storage scheme enables full duplex signal processing. It also shows that potential back-reflections which can occur in complex integrated circuits that consist of many discreet components are not distorting the delay process.
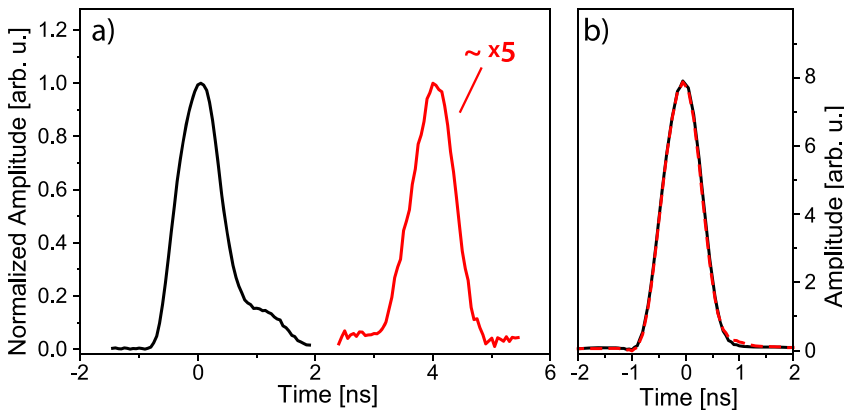

Figure 4: Nonreciprocal light storage. (a) Optical data pulses (black trace) propagating in one direction are delayed by 4 ns (red trace), whereas (b) simultaneously counterpropagating data pulses are not impacted (black trace shows transmitted data without delay applied to the counterpropagating signals, red dotted trace shows transmitted data while counterpropagating data are stored). Note that the readout efficiency of the pulses presented in (a) is around 20% and the data pulses are normalized to visualize the pulse shape before and after the storage process.
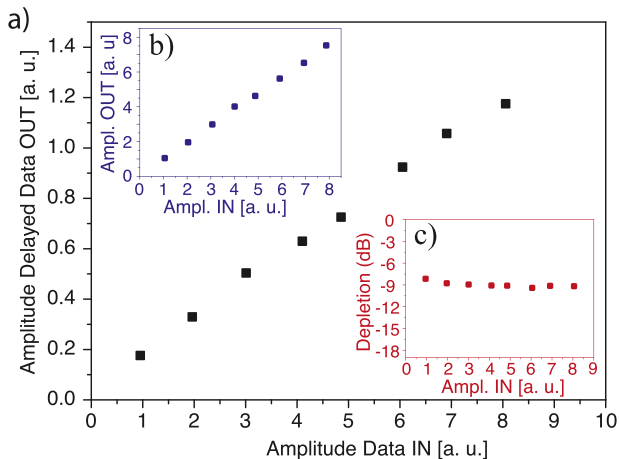
a)

Figure 5: Linearity of nonreciprocal light storage.
(a) Linear amplitude response of the delayed optical data pulses.
Inset (b) shows the linearity of the counterpropagating data pulses, whereas inset (c) shows the depletion of the data pulses for different input amplitude levels.

A crucial metric for nonreciprocal devices in general, which is particularly important for optical signal processing applications, is the linearity of the scheme. The linearity ensures that information encoded in the amplitude is maintained during the signal processing operation. Figure 5 shows that the Brillouin-based nonreciprocal delay scheme is linear over a wide range. The coupled power of the input data pulses in Figure 5 is varied by an order of magnitude from −10 to −20 dBm average optical power and we observe a linear relationship between input and output amplitude. We confirm that the same is true for the counterpropagating data channel (Figure 5b). The second inset, Figure 5c, shows that the depletion of the original data pulses which are transferred to the acoustic wave is approximately constant in the measured data power range.

3 Conclusion and outlook

We showed a nonreciprocal delay scheme based on the coherent interaction of photons with traveling acoustic phonons. The phase-matching underlying this process ensures that only optical data pulses traveling in a distinct direction are delayed. We showed that the bandwidth of this scheme is not limited to the intrinsic linewidth of the opto-acoustic interaction, but can, in fact, be much broader approaching the GHz regime. Furthermore, we demonstrated that the scheme depends linearly on the input power and does neither convert the optical mode nor the wavelength of the signal. Hence, it opens a pathway to full duplex signal processing architectures that can greatly reduce size,

weight, and power requirements. The delay time is continuously tunable as it is given by the difference in the arrival time of the readout pulse with respect to the write pulse within the phonon lifetime [32]. Recently, however, it was proposed and experimentally shown that the storage time can be extended by refreshing the acoustic phonon with optical pulses [45] overcoming said limitation.

Our demonstration of delaying an optical signal while another optical signal at the same frequency is counter-propagating shows the immunity of the here-presented delay scheme to detrimental back-reflections common in complex integrated photonic circuits that are composed of a multitude of optical elements. In the context of phased array antennas and beam steering elements, inducing nonreciprocal delays could enable new ways of separating transmitted and received signals.

4 Materials and methods

4.1 Experimental setup for nonreciprocal light storage

A layout of the experimental setup is shown in Figure 6.

As a laser source, we use a narrow-linewidth distributed feedback laser (TerraXion NLL) with a wavelength of around 1550 nm. The laser signal is divided into two arms, the data and the write/read arm. The data signal is up-shifted in frequency by the Brillouin frequency shift Ω via a single-sideband modulator. A single laser source is used to avoid relative drift of the data and the write/read arm. Two intensity modulators connected to a multichannel arbitrary waveform generator are used to chop the CW laser signals in both arms into a pulse stream. The write/read pulses are amplified via an erbium-doped fiber amplifier (EDFA) and afterward pass through a nonlinear fiber loop. The nonlinear fiber loop only transmits the write/read pulses and suppresses any background present from the laser or amplifier between the pulses as only the pulses have a high enough intensity to induce a nonlinear phase shift in the fiber loop. Hence, only the pulses are transmitted and the low-intensity background is reflected by the loop. A second EDFA after the loop boosts the signal to peak powers of several Watts. To minimize the effect of white noise, bandpass filters with a bandwidth of around 0.5 nm are implemented after every amplification step by the EDFAs. The one-laser setup, the low-noise EDFA combined with filtering, and the nonlinear loop are all used in the setup to maximize the signal-to-noise ratio that ensures the highest efficiency of the storage process with the least amount of distortions. The write and read pulses are coupled into the photonic chip using lensed fibers and the average coupled on-chip power was around 7 dBm.

The data signal is split with a 50/50 coupler and coupled from both sides into the photonic chip with an average power of around −10 dBm. From one side, the write/read pulses are combined with the data pulses and coupled via the same lensed fiber into the chip. Additional 50/50 couplers are used in the data path to make sure the data pulses and the write/read pulses overlap in the middle of the waveguide. Circulators are used on both sides of the chip to route the transmitted data signal to a two-channel fast oscilloscope. Two
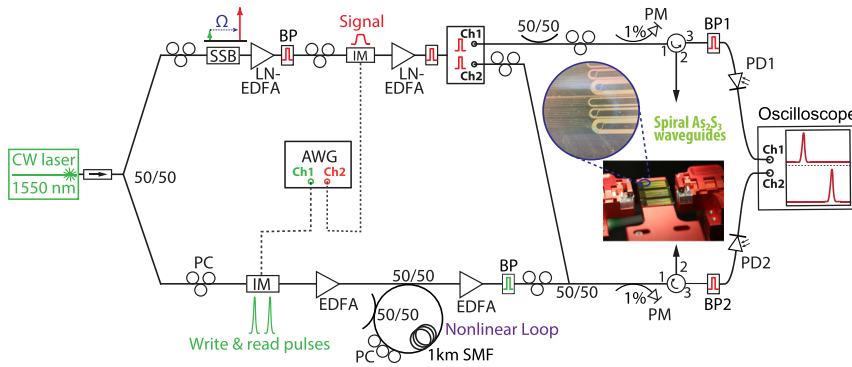
Figure 6: Experimental setup. Continuous wave (CW) laser, continuous-wave laser; 50/50: 50/50 optical fiber coupler; PC, polarization controller; SSB, single-sideband modulator; EDFA, erbium-doped fiber amplifier; LN-EDFA, low-noise EDFA; IM, intensity modulator; BP, bandpass filter; AWG, arbitrary waveform generator; CH 1/2, Channel 1/2; SMF, standard single-mode fiber; PM, power meter; PD, photodetector.

narrowband filters with a bandwidth of 3 GHz are used before the fast photodetectors (bandwidth 12 GHz) to filter residual write/read pulses.

4.2 Storage medium

The storage medium for the nonreciprocal light storage is a chalcogenide rib waveguide [37, 46]. The chalcogenide As_2S_3 thin film of around 850 nm is deposited on a thermal oxide silicon wafer with a variation of the film thickness below 5% [47]. Photolithography is used to pattern the waveguide structures which are etched into the thin film using inductively coupled plasma dry etching with a mixture of CHF_3, O_2, and Ar. The dimensions of the rib structure are 850 nm by 2.2 µm with a 50% etch depth and an overall length of 22 cm. The waveguide is arranged in a spiral to reduce the overall footprint to around 16 mm². The bend radius of the spiral is around 200 µm to ensure that there is no additional bending loss introduced for the fundamental optical mode as well as the acoustic mode.

The chalcogenide glass As_2S_3 is sandwiched between a silica substrate and a silica top-cladding to ensure guiding of the acoustic as well as the optical mode [36]. The difference in refractive index of silica $n \approx 1.4$ and the chalcogenide rib waveguides $n \approx 2.4$ guarantees tight confinement of the optical mode, whereas the difference in sound velocity of around 3400 m/s prevents leakage of the acoustic mode into the substrate or cladding which enables strong overlap between the two respective modes. The silica top-cladding is deposited using sputtering.

Light is coupled in and out of the chip using lensed fibers with a roughly 2 µm focus spot size. The coupling loss per facet is around 4 dB. The polarization is adjusted so light is coupled into the fundamental TE mode of the waveguide which is the mode with the lowest loss.

Author contributions: All the authors have accepted responsibility for the entire content of this submitted manuscript and approved submission.

Conflict of interest statement: The authors declare no conflicts of interest regarding this article.

References

[1] D. Jalas, A. Petrov, M. Eich, et al., "What is – and what is not – an optical isolator," *Nat. Photonics*, vol. 7, pp. 579–582, 2013.

[2] D. L. Sounas and A. Alù, "Non-reciprocal photonics based on time modulation," *Nat. Photonics*, vol. 11, pp. 774–783, 2017.

[3] C. Caloz, A. Andrea, S. Tretyakov, D. Sounas, K. Achouri, and Z. L. Deck-Léger, "Electromagnetic nonreciprocity," *Phys. Rev. Appl.*, vol. 10, p. 1, 2018.

[4] Y. Shoji, T. Mizumoto, H. Yokoi, I. Wei Hsieh, and R. M. Osgood, "Magneto-optical isolator with silicon waveguides fabricated by direct bonding," *Appl. Phys. Lett.*, vol. 92, pp. 2–5, 2008.

[5] L. Bi, J. Hu, P. Jiang, et al., "On-chip optical isolation in monolithically integrated non-reciprocal optical resonators," *Nat. Photonics*, vol. 5, pp. 758–762, 2011.

[6] D. Huang, P. Pintus, C. Zhang, et al., "Dynamically reconfigurable integrated optical circulators," *Optica*, vol. 4, p. 23, 2017.

[7] Z. Yu and S. Fan, "Complete optical isolation created by indirect interband photonic transitions," *Nat. Photonics*, vol. 3, pp. 91–94, 2009.

[8] H. Lira, Z. Yu, S. Fan, and M. Lipson, "Electrically driven nonreciprocity induced by interband photonic transition on a silicon chip," *Phys. Rev. Lett.*, vol. 109, pp. 1–5, 2012.

[9] M. S. Kang, A. Butsch, and P. S. J. Russell, "Reconfigurable light-driven opto-acoustic isolators in photonic crystal fibre," *Nat. Photonics*, vol. 5, pp. 549–553, 2011.

[10] D. B. Sohn, S. Kim, and G. Bahl, "Time-reversal symmetry breaking with acoustic pumping of nanophotonic circuits," *Nat. Photonics*, vol. 12, pp. 91–97, 2018.

[11] E. Verhagen and A. Alù, "Optomechanical nonreciprocity," *Nat. Phys.*, vol. 13, pp. 922–924, 2017.

[12] M. Ali Miri, F. Ruesink, E. Verhagen, and A. Alù, "Optical nonreciprocity based on optomechanical coupling," *Phys. Rev. Appl.*, vol. 7, pp. 1–20, 2017.

[13] S. Manipatruni, J. T. Robinson, and M. Lipson, "Optical nonreciprocity in optomechanical structures," *Phys. Rev. Lett.*, vol. 102, p. 213903, 2009.

[14] M. Hafezi and P. Rabl, "Optomechanically induced non-reciprocity in microring resonators," *Optic Express*, vol. 20, p. 7672, 2012.

[15] X. W. Xu and Y. Li, "Optical nonreciprocity and optomechanical circulator in three-mode optomechanical systems," *Phys. Rev. A Atom. Mol. Opt. Phys.*, vol. 91, pp. 1–8, 2015.

[16] F. Ruesink, M.-A. Miri, A. Alù, and E. Verhagen, "Nonreciprocity and magnetic-free isolation based on optomechanical interactions," *Nat. Commun.*, vol. 7, p. 13662, 2016.

[17] Z. Shen, Y.-L. Zhang, Y. Chen, et al., "Experimental realization of optomechanically induced non-reciprocity," *Nat. Photonics*, vol. 10, pp. 657–661, 2016.

[18] K. Fang, J. Luo, A. Metelmann, et al., "Generalized non-reciprocity in an optomechanical circuit via synthetic magnetism and reservoir engineering," *Nat. Phys.*, vol. 13, pp. 465–471, 2017.

[19] Z. Shen, Y.-L. Zhang, Y. Chen, et al., "Reconfigurable optomechanical circulator and directional amplifier," *Nat. Commun.*, vol. 9, p. 1797, 2018.

[20] N. A. Estep, D. L. Sounas, and A. Alù, "Magnetless microwave circulators based on spatiotemporally modulated rings of coupled resonators," *IEEE Trans. Microw. Theor. Tech.*, vol. 64, pp. 502–518, 2016.

[21] G. A. Peterson, F. Lecocq, K. Cicak, R. W. Simmonds, J. Aumentado, and J. D. Teufel, "Demonstration of efficient nonreciprocity in a microwave optomechanical circuit," *Phys. Rev. X*, vol. 7, p. 031001, 2017.

[22] S. Barzanjeh, M. Wulf, M. Peruzzo, et al., "Mechanical on-chip microwave circulator," *Nat. Commun.*, vol. 8, p. 953, 2017.

[23] N. R. Bernier, L. D. Tóth, A. Koottandavida, et al., "Nonreciprocal reconfigurable microwave optomechanical circuit," *Nat. Commun.*, vol. 8, 2017. https://doi.org/10.1038/s41467-017-00447-1.

[24] X. Huang and S. Fan, "Complete all-optical silica fiber isolator via stimulated Brillouin scattering," *J. Lightwave Technol.*, vol. 29, pp. 2267–2275, 2011.

[25] B. J. Eggleton, C. G. Poulton, P. T. Rakich, M. J. Steel, and G. Bahl, "Brillouin integrated photonics," *Nat. Photonics*, vol. 13, pp. 664–677, 2019.

[26] C. G. Poulton, R. Pant, A. Byrnes, S. Fan, M. J. Steel, and B. J. Eggleton, "Design for broadband on-chip isolator using stimulated Brillouin scattering in dispersion-engineered chalcogenide waveguides," *Opt. Express*, vol. 20, p. 21235, 2012.

[27] E. A. Kittlaus, N. T. Otterstrom, P. Kharel, S. Gertler, and P. T. Rakich, "Non-reciprocal interband Brillouin modulation," *Nat. Photonics*, vol. 12, pp. 613–620, 2018.

[28] J. H. Kim, M. C. Kuzyk, K. Han, H. Wang, and G. Bahl, "Non-reciprocal Brillouin scattering induced transparency," *Nat. Phys.*, vol. 11, pp. 275–280, 2015.

[29] C.-H. Dong, Z. Shen, C.-L. Zou, Y.-L. Zhang, W. Fu, and G.-C. Guo, "Brillouin-scattering-induced transparency and non-reciprocal light storage," *Nat. Commun.*, vol. 6, p. 6193, 2015.

[30] J. H. Kim, S. Kim, and G. Bahl, "Complete linear optical isolation at the microscale with ultralow loss," *Sci. Rep.*, vol. 7, pp. 1–9, 2017.

[31] R. W. Boyd, *Nonlinear Optics*, Acad. Press, 2003.

[32] M. Merklein, B. Stiller, K. Vu, S. J. Madden, and B. J. Eggleton, "A chip-integrated coherent photonic–phononic memory," *Nat. Commun.*, vol. 8, p. 574, 2017.

[33] B. Stiller, M. Merklein, K. Vu, et al., "Cross talk-free coherent multi-wavelength Brillouin interaction," *APL Photonics*, vol. 4, p. 040802, 2019.

[34] Z. Zhu, D. J. Gauthier, and R. W. Boyd, "Stored light in an optical fiber via stimulated Brillouin scattering," *Science*, vol. 318, pp. 1748–50, 2007.

[35] M. Merklein, B. Stiller, and B. J. Eggleton, "Brillouin-based light storage and delay techniques," *J. Opt.*, vol. 20, p. 083003, 2018.

[36] C. G. Poulton, R. Pant, and B. J. Eggleton, "Acoustic confinement and stimulated Brillouin scattering in integrated optical waveguides," *J. Opt. Soc. Am. B*, vol. 30, pp. 2657–2664, 2013.

[37] R. Pant, C. G. Poulton, D.-Y. Choi, et al., "On-chip stimulated Brillouin scattering," *Opt. Express*, vol. 19, pp. 8285–8290, 2011.

[38] V. Fiore, Y. Yang, M. C. Kuzyk, R. Barbour, L. Tian, and H. Wang, "Storing optical information as a mechanical excitation in a silica optomechanical resonator," *Phys. Rev. Lett.*, vol. 107, pp. 1–5, 2011.

[39] V. Fiore, C. Dong, M. C. Kuzyk, and H. Wang, "Optomechanical light storage in a silica microresonator," *Phys. Rev.*, vol. 87, p. 023812, 2013.

[40] Y. Okawachi, M. Bigelow, J. Sharping, et al., "Tunable all-optical delays via Brillouin slow light in an optical fiber," *Phys. Rev. Lett.*, vol. 94, p. 153902, 2005.

[41] K. Y. Song, M. Herráez, and L. Thévenaz, "Observation of pulse delaying and advancement in optical fibers using stimulated Brillouin scattering," *Opt. Express*, vol. 13, pp. 82–88, 2005.

[42] K. Y. Song, K. Lee, and S. B. Lee, "Tunable optical delays based on Brillouin dynamic grating in optical fibers," *Opt Express*, vol. 17, pp. 10344–9, 2009.

[43] S. Preussler, K. Jamshidi, A. Wiatrek, R. Henker, C.-A. Bunge, and T. Schneider, "Quasi-light-storage based on time-frequency coherence," *Opt Express*, vol. 17, pp. 15790–15798, 2009.

[44] S. Chin and L. Thévenaz, "Tunable photonic delay lines in optical fibers," *Laser Photonics Rev.*, vol. 6, pp. 724–738, 2012.

[45] B. Stiller, M. Merklein, C. Wolff, et al., "Coherently refreshing hypersonic phonons for light storage," *Optica*, vol. 7, p. 492, 2020.

[46] S. J. Madden, D.-Y. Choi, D. A. Bulla, et al., "Long, low loss etched As(2)S(3) chalcogenide waveguides for all-optical signal regeneration," *Opt. Express*, vol. 15, pp. 14414–14421, 2007.

[47] A. Zarifi, B. Stiller, M. Merklein, et al., "Highly localized distributed Brillouin scattering response in a photonic integrated circuit," *APL Photonics*, vol. 3, p. 036101, 2018.